Rigidity generation by nonthermal fluctuations

R. Sheshka,[1] P. Recho,[2,3] and L. Truskinovsky[4,5,*]

[1]*LITEN, CEA-Grenoble, 17 rue des Martyrs, 38054 Grenoble, France*
[2]*Mathematical Institute, University of Oxford, Oxford OX26GG, United Kingdom*
[3]*Engineering Department, University of Cambridge, Cambridge CB2 1PZ, United Kingdom*
[4]*LMS, CNRS-UMR 7649, École Polytechnique, 91128 Palaiseau, France*
[5]*Physique et Mecanique des Milieux Heterogenes CNRS – UMR 7636 ESPCI ParisTech 10 Rue Vauquelin, 75005 Paris, France*

Active stabilization in systems with zero or negative stiffness is an essential element of a wide variety of biological processes. We study a prototypical example of this phenomenon and show how active rigidity, interpreted as a formation of a pseudowell in the effective energy landscape, can be generated in an overdamped stochastic system. We link the transition from negative to positive rigidity with time correlations in the additive noise, and we show that subtle differences in the out-of-equilibrium driving may compromise the emergence of a pseudowell.

I. INTRODUCTION

The response of biological systems to mechanical loading depends not only on the load bearing properties of their constituents, their connectivity and the temperature, but also on the presence of nonthermal endogenous driving. For instance, ATP-driven molecular motors can both stiffen the cytoskeleton and fluidize it [1–4]. While it is clear that the nonequilibrium environment modifies the nature of the statistical forces acting in driven systems, the mesoscale thermomechanics of such systems is not well understood, even in the case of steady states [5–7].

At the level of a single cell, active rigidity may be the outcome of tensegrity-type tightening [8], connectivity change [9], steric interactions [10], or a general motor-induced prestress coupled with extreme nonlinearity of the passive response [11,12]. An example of ATP-induced stiffening at larger scales is the Frank-Starling effect in cardiac muscles, which cannot be explained by a simple filament overlap change [13].

One of the most striking effects of active rigidity is the stable mechanical functioning of the systems with negative passive stiffness, as in the case of hair cells [14–16] and muscle half-sarcomeres [17–19]. In these and other similar systems, metabolic resources are used to modify the mechanical susceptibility of the system and stabilize configurations that would not have existed in the absence of ATP hydrolysis [20–22].

The goal of this paper is to study the effect of an internal driving on the pseudoelastic moduli that characterize the slow mechanical response of active systems [23]. We show that active rigidity, or, more generally, active susceptibility, can emerge at the microscale through resonant nonthermal excitation of molecular degrees of freedom. Our inspiration comes from the inverted Kapitza pendulum [24], except that in biological systems the inertial stabilization has to be replaced by its overdamped analog. In both cases, however, the macroscopic mechanical stiffness can be controlled by a time-correlated noise, which in a biological setting may serve as a mechanical representation of a nonequilibrium chemical reaction [25].

In the interest of analytical transparency, we limit our attention to mean-field systems that can be described by a single degree of freedom. In such systems, active stabilization can be viewed as a creation of a noise-induced pseudowell in an effective energy landscape. The proposed mechanism of rigidity generation requires a finite distance from thermodynamic equilibrium and is therefore different from conventional entropic stabilization, which operates, for instance, in rubber elasticity [26] and serves for stabilization of body-centered-cubic (bcc) structures [27]. Our main result is that the emergence of pseudowells is not an automatic consequence of the violation of detailed balance but is a phenomenon that is highly sensitive to the fine stochastic signature of the nonequilibrium driving.

To justify our mean-field model, we consider in some detail the case of skeletal muscle cells [28], where we neglect the detachment of active cross-linkers (cross-bridges) and model an elementary series element (half-sarcomere) as a parallel array of molecular motors operating in stall conditions. Due to the rigid connection between elements, the interactions in this system are of long-range type, which is responsible for negative passive stiffness of half-sarcomeres in physiologically relevant conditions [19,29–31]. This creates a stability problem for a myofibril, given that it can be viewed as a series connection of half-sarcomeres, and one of the goals of our paper is to link the stability of affine configurations in this system [32,33] with the presence of directionless endogenous noise fueled by ATP hydrolysis.

More specifically, we model attached myosin motors as bistable springs, with two energy wells corresponding to pre- and post-power-stroke configurations. Each "snap-spring" of this kind acts against a linear spring, representing a structural filament. The system is exposed to both uncorrelated agitation (scaled with temperature-type parameter D) and a correlated noise representing ATP hydrolysis (scaled with affinity-type parameter A).

Building upon the idea of active drift [34], we consider a family of stall states in this system parametrized by a

_____

[*]lev.truskinovsky@espci.fr

mesoscopic measure of the total deformation. We compute the time- and ensemble-averaged potential at the fixed value of the deformation parameter, and we interpret the deformation derivative of this potential as an effective stiffness. We show that a nonequilibrium phase diagram in the space of parameters (D,A) exhibits three different dynamic phases, including the one associated with the activity-induced pseudoenergy well. The overall behavior of the model is controlled by a tricritical point with transitions of second order due to entropic stabilization and of first order due to active stabilization.

We systematically study the sensitivity of the phenomenon of active stabilization to the stochastic nature of the nonequilibrium reservoir. We show that while in periodic (P) or dichotomous (DC) environments, the pseudowell exists in an extended domain of the parameter space; active stabilization disappears if the noise is of Ornstein-Uhlenbeck (OU) type. The sensitive dependence of the mechanical performance of the molecular scale devices on the shape of the power spectrum of the noise was observed in some studies of active drift [35,36], and here we broaden the picture by covering molecular machines generating active rigidity. Various features captured by our minimal model are in common not only with inertial stabilization [24], but also with the performance of the Ising model in periodic magnetic field [37], the folding/unfolding of proteins subjected to periodic forces [38], and the parametric behavior of more complex actively driven systems [39–41].

The paper is organized as follows. In Sec. II we introduce the simplest zero-dimensional system exhibiting active stabilization, and we justify it from the perspective of muscle mechanics. In Sec. III we study numerically the finite-temperature behavior of the system subjected to three different types of nonequilibrium driving: P, DC, and OU. The analytically transparent zero-temperature limits in all three problems are presented separately in Sec. IV. Our conclusions are summarized in Sec. V. A short announcement of our main results can be found in Ref. [42].

II. THE PROBLEM

We begin with a formal justification of a prototypical model that we later study in full detail. While it schematizes a broad class of active phenomena in endogenously driven nonequilibrium systems, in this paper we justify it in the context of mean-field modeling of muscle half-sarcomeres [43].

A. Mean-field model

As in typical experiments [3,4,25,44], we consider a probe characterized by a (microscopic) coordinate x and placed in an active environment. The probe is attached through an elastic spring to a measuring device characterized by a (mesoscopic) variable y. We assume that the variable y is slow and treat it as a control parameter. Instead, the variable $x(t)$ will undergo fast stochastic motion that will have to be averaged out.

In the absence of noise, the environment will be characterized by the potential $V(x)$, and we assume that the probe is placed in an unstable configuration. One way to satisfy this condition is to assume that $V(x)$ has a double-well structure with the reference position of a probe in a spinodal state. We further assume that the probe is exposed to a fluctuating surrounding medium with a quickly relaxing component represented by an equilibrium thermostat and a relatively slower relaxing component describing a nonequilibrium environment. We study the mesoscopic force exerted by the probe on the measuring device, which implies the transition from the environment potential $V(x)$ to the effective potential for the measuring device $F(y)$.

To be specific, consider the stochastic dynamics of a variable $x(t)$ described by a dimensionless Langevin equation,

$$\dot{x} = -\partial_x E(x,y,t) + \sqrt{2D}\xi(t), \tag{1}$$

where $\xi(t)$ is a standard white noise and D is a temperature-like characteristic of the equilibrium thermostat. The potential $E(x,y,t) = E_{\mathrm{p}}(x,t) + E_{\mathrm{m}}(x,y)$ is a sum of two components: $E_{\mathrm{p}}(x,t) = V(x) - xf(t)$, describing the probe in an out-of-equilibrium environment, and $E_{\mathrm{m}}(x,y) = k(x - y)^2/2$, describing the linear elastic coupling with a measuring device characterized by stiffness k. We assume that the energy is supplied to the system through the rocking force $f(t)$ with zero average, which is characterized by an amplitude A and a time scale τ. To obtain analytical results, we need to assume further that the potential $V(x)$ is biquadratic,

$$V(x) = (|x| - 1/2)^2/2. \tag{2}$$

A similar framework has been used before in the studies of directional motion of molecular motors [35].

To compute the effective potential $F(y)$, we use an observation that if the "measurements" are performed at a time scale larger that τ, the resulting force is $T(y) = k[y - \overline{\langle x \rangle}]$, where the averaging is over the ensemble and time,

$$\overline{\langle x \rangle} = \lim_{t \to \infty} (1/t) \int_0^t \int_{-\infty}^{\infty} x p(x,t) dx \, dt.$$

Here $p(x,t)$ is the probability distribution for the variable x, which solves an associated Fokker-Plank equation. The primitive of the averaged tension,

$$F(y) = \int^y T(s) ds, \tag{3}$$

can then be viewed as a nonequilibrium analog of the free energy [45–48]. While in our case the mean-field nature of the model ensures potentiality of the averaged tension, in a more general setting the averaged stochastic forces will lose their gradient structure, and even the effective "equations of states" relating averaged forces with the corresponding generalized coordinates may not be well defined [7,49–53].

It is clear that the effective potential $F(y)$ will depend not only on $V(x)$ but also on the stochastic properties of the driving $f(t)$. The question we pose is whether there exists a nonbiased stochastic driving that ensures stabilization of spinodal configurations that would be unstable in the absence of the noise. In the equilibrium case, when $f(t) = 0$, such stabilization is possible because of entropic effects but only at sufficiently large temperature D. The challenge is to find a correlated (colored) noise $f(t)$ that ensures stabilization at arbitrarily small D. The possibility of bimodality of the marginal probability distribution $p(x,t)$ in single-well potentials is known for DC and Levi-type noises [54,55], however this effect disappears after ensemble-averaging involved in the computation of the effective potential $F(y)$.
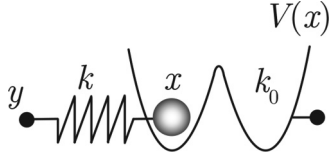
FIG. 1. Schematic representation of a bistable snap-spring in series with a linear spring.

Before we turn to the systematic study of the prototypical problem (1), we present in the next section a justification of this model from the viewpoint of the microscopic multibody mechanics of skeletal muscles. In the case of muscles, the mean-field interactions are due to the presence of parallel connections between actomyosin cross-bridges realized through relatively rigid myosin backbones [19].

B. Microscopic problem

According to Huxley-Simmons theory [43], individual half-sarcomeres in skeletal muscles with attached cross-bridges can be expected to operate in an unstable (spinodal) or near-critical regime [18,19]. This warrants strain inhomogeneities at the level of a myofibril [32,33] that have not been systematically observed. Purely entropic stabilization is excluded in this case because the temperature alone is not sufficiently high to ensure positive stiffness of individual half-sarcomeres [18]. Here we discuss a possibility that the relative homogeneity of the myofibril deformation is due to active stabilization of individual half-sarcomeres.

Following [18,43], we present a myofibril as a chain of half-sarcomeres arranged in series with each half-sarcomere represented by a parallel array of N cross-bridges interacting with a single actin filament; see Fig. 2. We assume that the nontrivial dynamics of attached cross-bridges is due exclusively to the conformational change in myosin heads (power stroke) and model cross-bridges as bistable elements in series with linear springs; see Fig. 1. We further assume that the nonequilibrium driving is provided through the rocking of the bistable elements [56].

A half-sarcomere in this model [see Fig. 2(b)] can be described by the system of nondimensional Langevin equations

$$dx_i/dt = -\nabla_{x_i}\Phi + \sqrt{2D}\xi(t),$$
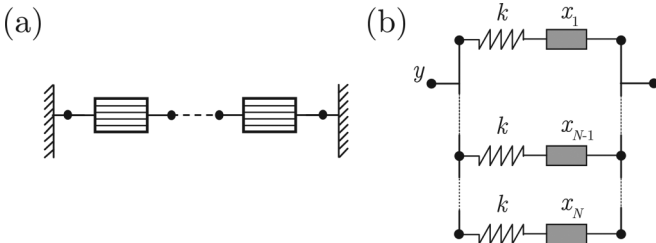$$\nu dy/dt = -\nabla_y\Phi, \qquad (4)$$

FIG. 2. (a) Schematic representation of a muscle myofibril as a series connection of half sarcomeres; (b) model of a single half-sarcomere with attached cross-bridges arranged in parallel. Shaded boxes in (b) represent bistable snap-springs shown in Fig. 1.

where y is a macroscopic variable characterizing the strain at the level of the half-sarcomere whose dynamics is slow due to the large value of the relative viscosity ν. The variable y is coupled with N fast soft-spin-type variables x_i through identical springs with stiffness k. The potential energy is $\Phi = \sum_{i=1}^{N} E(x_i,y,t) - f_{\text{ext}}y$, where $f_{\text{ext}}(t)$ is a slowly varying macroscopic force. The ensuing problem is a soft-spin generalization [29] of the Huxley-Simmons model [43], and its applications are known to extend far beyond muscles mechanics, from hair cell gating [15] and binding of cell-adhesion patches [57] to mechanical denaturation of RNA and DNA hairpins [58] and unzipping of biological macromolecules [59].

The equation for y in Eq. (4) can be rewritten as

$$\frac{\nu}{N}\frac{dy}{dt} = k\left(\frac{1}{N}\sum_{i=1}^{N}x_i - y\right) + \frac{f_{\text{ext}}}{N}, \qquad (5)$$

which makes the mean-field nature of the interaction between y and x_i explicit. If N is large, we can replace $\frac{1}{N}\sum_{i=1}^{N}x_i$ by $\langle x\rangle$ using the fact that the variables x_i are identically distributed and exchangeable [60]. If $\nu_0 = \nu/N$ and $g_{\text{ext}} = f_{\text{ext}}/(kN)$ remain finite in the limit $N \to \infty$, we can write

$$\nu_0\frac{dy}{dt} = k[(\langle x\rangle - y) + g_{\text{ext}}(t)].$$

Assume for determinacy that the function $f(t)$ is periodic and choose its period τ in such a way that $\Gamma = \nu_0/k \gg \tau$. Since $g_{\text{ext}}(t)$ is a slowly varying function at the time scale τ, we can split the force $k(\langle x\rangle - y)$ acting on y into a slow component $k\psi(y) = k(\overline{\langle x\rangle} - y)$, which originates from our effective potential, and a slow-fast component $k\phi(y,t) = k(\langle x\rangle - \overline{\langle x\rangle})$, which in the steady regime becomes a τ periodic function of time with zero average. We can then write

$$\Gamma\frac{dy}{dt} = \psi(y) + \phi(y,t) + g_{\text{ext}}. \qquad (6)$$

The next step is to average (6) over the time scale τ. Toward that end, we introduce a decomposition $y(t) = z(t) + \zeta(t)$, where z is the averaged (slow) part of the motion and ζ is a fast varying perturbation (with time scale τ) that is small compared to z. Then, expanding (6) up to first order in ζ, we obtain

$$\Gamma\left(\frac{dz}{dt} + \frac{d\zeta}{dt}\right)$$
$$= \psi(z) + \partial_z\psi(z)\zeta + \phi(z,t) + \partial_z\phi(z,t)\zeta + g_{\text{ext}}. \qquad (7)$$

Since $g_{\text{ext}}(t) \simeq \tau^{-1}\int_t^{t+\tau} g_{\text{ext}}(u)du$, we obtain at a fast time scale [61]

$$\Gamma\frac{d\zeta}{dt} = \phi(z,t).$$

Integrating this equation between t_0 and $t \leqslant t_0 + \tau$, we can assume that z is fixed and therefore $\zeta(t) - \zeta(t_0) = \Gamma^{-1}\int_{t_0}^{t}\phi(z(t_0),u)du$. Given that ϕ is τ-periodic with zero average, we conclude that $\zeta(t)$ is also τ-periodic with zero average.

If we now average (7) over the fast time scale τ, we obtain

$$\Gamma dz/dt = \psi(z) + r + g_{\text{ext}},$$

where

$$r = (\Gamma\tau)^{-1} \int_0^\tau \int_0^t \partial_z\phi(z,t)\phi(z,u)du\,dt.$$

Since both $\phi(z,t)$ and $\partial_z\phi(z,t)$ are bounded, we can write $|r| \leqslant (\tau/\Gamma)c \ll 1$, where the "constant" c depends on z but not on τ and Γ. Therefore, if $N \gg 1$ and $\nu/(kN) \gg \tau$, the equation for

$$z(t) = \tau^{-1} \int_t^{t+\tau} y(u)du$$

can be written directly in terms of the effective potential introduced in Eq. (3)

$$(\nu/N)\dot{z} = -\partial_z F + f_{\text{ext}}/N.$$

To find the potential $F(z)$, we need to average over the fast and slow-fast dynamics in Eq. (1) while keeping the variable y fixed.

C. Nondimensionalization

Equation (1), which constitutes the basis of our prototypical model, is dimensionless. To translate the results back into the context of muscles, we need to use the time scale $\tau^\star = \eta/k_0 \sim 0.1$ ms, where $\eta \sim 0.38$ ms. pN/nm is the microscale viscosity [19] and $k_0 \sim 3$ pN/nm is the passive stiffness of the equivalent energy wells. The spatial scale is then $l^\star = a$, where $a \sim 10$ nm is the distance between two minima of the pre- and post-power-stroke wells [62] and the energy scale is $\epsilon^\star = k_0 a^2 \sim 300$ pN nm.

Following [19], we also assume that $k = k_m/k_0 \sim 0.6$, where $k_m \sim 2$ pN/nm is the stiffness of the elastic part of the myosin motor [63,64]. Hence $D = k_B\Theta/(k_0a^2) \sim 0.01$, where $k_B = 4.10$ pN nm is the Boltzmann constant, $\Theta \sim 300$ K is the ambient temperature, and $a = 10$ nm is the characteristic size of a motor power-stroke [62]. For the active driving, we obtain $\tau = \tau_a/(\eta/k_0) \sim 100$, where $\tau_a = 40$ ms is the characteristic time of ATP hydrolysis [28]. We can now write that $A = \sqrt{\Delta\mu/(k_0a^2)} \approx 0.5$, where $\Delta\mu = 20k_B\Theta$ is the typical value of the degree of nonequilibrium in terms of the affinity of the ATP hydrolysis reaction [28].

The knowledge of the set of dimensionless parameters A, D, and τ will be sufficient to locate the muscle system on the phase (regime) diagram. Such diagrams will be constructed in Sec. III for three different types of active driving.

III. PHASE DIAGRAMS

In this section, we consider the general problem (1) at finite temperature ($D > 0$) when both equilibrium and nonequilibrium reservoirs are contributing to the microscopic dynamics simultaneously. The limiting case of zero temperatures ($D = 0$) will be analyzed separately in Sec. IV.

A. Periodic (P) driving

Suppose first that the nonequilibrium driving is represented by a periodic (P) square-shaped external force $f(t) = A(-1)^{n(t)}$ with $n(t) = \lfloor 2t/\tau \rfloor$, where the brackets denote the integer part. While this choice of periodic driving ensures
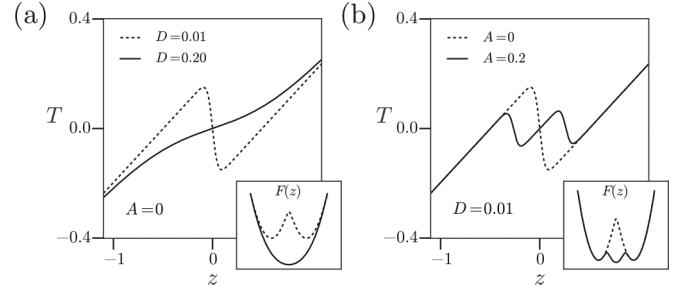

FIG. 3. Tension elongation curves $T(z)$ in the case of periodic driving (adiabatic limit). The equilibrium system ($A = 0$) is shown in (a) and the out-of-equilibrium system ($A \neq 0$) is shown in (b). The insets show the effective potential $F(z)$. Here $k = 0.6$.

a certain analytical simplicity, the obtained results will be generic.

It will be convenient to rewrite the dynamic equation (1) in the form

$$\frac{dx}{dt} = -\partial_x \tilde{V}(x,z) + f(t) + \sqrt{2D}\xi(t), \quad (8)$$

where

$$\tilde{V}(x,z) = \tfrac{1}{2}(|x| - 1/2)^2 + \tfrac{1}{2}k(x-z)^2.$$

The associated Fokker-Planck equation for the time-dependent probability distribution $p(x,t)$ reads

$$\partial_t p = \partial_x[p\partial_x E(x,t) + D\partial_x p]. \quad (9)$$

First of all, we note that an explicit solution of (9) can be found in the adiabatic case when the correlation time τ is much larger than the escape time for the bistable potential V [65,66]. The idea of this approximation is that the time average of the steady-state probability can be computed from the mean of the stationary probabilities with constant driving force [either $f(t) = A$ or $f(t) = -A$]. The domain of applicability of the adiabatic approximation in the case of bi-quadratic potential is discussed in Appendix A.

It is obvious that the adiabatic approximation becomes exact in the special case of an equilibrium system with $A = 0$ when the stationary probability distribution is known explicitly:

$$p_0(x) = Z^{-1}e^{-\tilde{V}(x)/D},$$

where $Z = \int_{-\infty}^{\infty} \exp[-\tilde{V}(x)/D]dx$. The tension elongation curve can then be computed analytically, since we know

$$\overline{\langle x \rangle} = \langle x \rangle = \int_{-\infty}^{\infty} x p_0(x)dx$$

The resulting curve $T(z)$ and the corresponding potential $F(z)$ are shown in Fig. 3(a). At zero temperature the equilibrium system with $A = 0$ exhibits negative stiffness at $z = 0$ where the effective potential $F(z)$ has a maximum (spinodal state). As temperature increases, we observe a standard entropic stabilization of the configuration $z = 0$; see Fig. 3(a).

Computing the solution of the equation $\partial_z T|_{z=0} = 0$, we find an explicit expression for the critical temperature $D_e = r/[8(1 + k)]$, where r is a root of a transcendental equation
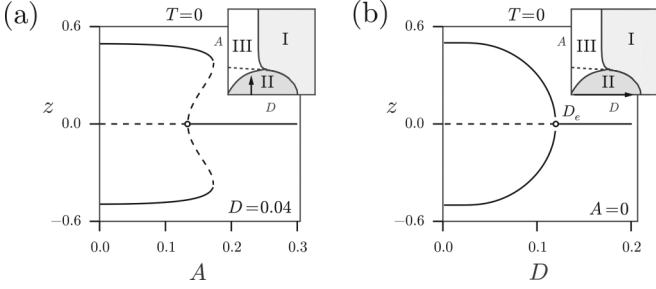
FIG. 4. The parameter dependence of the roots of the equation $T(z) = 0$ in the adiabatic limit: (a) fixed $D = 0.04$ and varying A, first-order phase transition [line $C_A - M_A$ in Fig. 5(a)]; (b) fixed $A = 0$ and varying D, second-order phase transition [line $D_e - C_A$ in Fig. 5(a)]. The dashed lines correspond to unstable branches. Here $k = 0.6$.
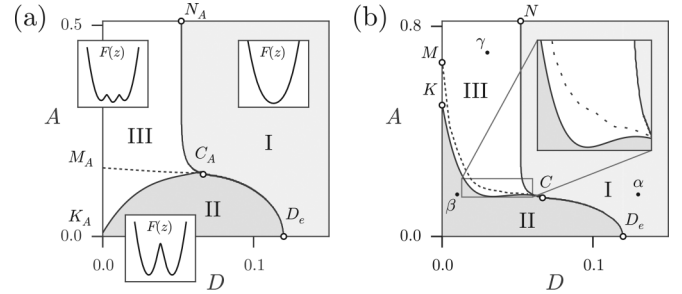

FIG. 5. Phase diagram in the (A, D) plane showing phases I, II, and III: (a) adiabatic limit, (b) numerical solution at $\tau = 100$ (b). C_A is the tricritical point, D_e is the point of a second-order phase transition in the passive system. The "Maxwell line" for a first-order phase transition in the active system is shown by dots. Here $k = 0.6$.

$1 + \sqrt{r/\pi}e^{-1/r}/[1 + \mathrm{erf}(1/\sqrt{r})] = r/(2k)$. The behavior of the roots of the equation $T(z) = -k(\langle x \rangle - z) = 0$ at $A = 0$ is shown in Fig. 4(b). It illustrates a second-order phase transition taking place at $D = D_e$.

In the case of constant force $f \equiv A$, the stationary probability distribution is also known [67],

$$p_A(x) = Z^{-1} e^{-(\tilde{V}(x) - Ax)/D},$$

where again $Z = \int_{-\infty}^{\infty} \exp[-\tilde{V}(x)/D] dx$. In the adiabatic approximation, we can write the time-averaged stationary distribution in the form $p_{\mathrm{ad}}(x) = \frac{1}{2}[p_A(x) + p_{-A}(x)]$, which gives

$$\overline{\langle x \rangle} = \frac{1}{2}[\langle x \rangle(A) + \langle x \rangle(-A)]. \tag{10}$$

In this equation, the expression for $\langle x \rangle(A)$ can be written explicitly as

$$\langle x \rangle(A) = Z^{-1} \sum_{i=1,2} P(u_i)[\sqrt{\pi} u_i \mathrm{erfc}(u_i) - (-1)^i e^{-u_i^2}],$$

where

$$P(u) = [D/(1+k)]e^{-\frac{1}{2D}\left(\frac{1}{4} + kz^2 - 2Du^2\right)},$$

$$u_{1,2} = (A \pm 1/2 + kz)/\sqrt{2D(1+k)},$$

$$Z = \sqrt{(1+k)\pi/(2D)} \sum_{i=1,2} P(u_i) \mathrm{erfc}[(-1)^i u_i],$$

and erfc is the complementary error function.

The force-elongation curves $T(z)$ and the corresponding potentials $F(z)$ obtained for $A \neq 0$ are shown in Fig. 3(b). It demonstrates the main effect: as the degree of nonequilibrium, characterized by A, increases, not only does the stiffness in the state $z = 0$ where the original double-well potential V had a maximum change from negative to positive, but also the effective potential $F(z)$ develops the third well around this point. We interpret this phenomenon as the emergence of active rigidity because the new equilibrium state becomes possible only at a finite value of the driving parameter A while the temperature parameter D can be arbitrarily small. The behavior of the roots of the equation $T(z) = -k(\overline{\langle x \rangle} - z) = 0$ at $A \neq 0$ is shown in Fig. 4(a). It illustrates the first-order phase transitions taking place at increasing A (and small fixed D).

The full steady-state regime map (dynamic phase diagram) summarizing the results obtained in the adiabatic approximation is presented in Fig. 5(a). There, the "paramagnetic" phase I describes the regimes where the effective potential $F(z)$ is convex, the "ferromagnetic" phase II is a bistability domain where the potential $F(z)$ has a double-well structure, and, finally, the "Kapitza" phase III is where the function $F(z)$ has three convex sections separated by two concave (spinodal) regions. Note that the boundaries of the domain occupied by phase III in this diagram are not defined by the number of roots of $T(z) = 0$, as is usually done in the study of magnetic systems, but by counting the number of effective "energy wells" linked to convexity properties of the whole effective potential $F(z)$.

In view of the structure of the bifurcation diagrams shown in Fig. 4, we can interpret the boundary $C_A - D_e$ separating phases I and II as a line of (zero force) second-order phase transitions and the dashed line $C_A - M_A$ as a Maxwell line for the (zero force) first-order phase transition; see Fig. 4. Then C_A can be interpreted as a tricritical point near which the system can be described by a nonequilibrium (active) Landau potential of the form

$$F(z) = F_0 + rz^2 + qz^4 + pz^6,$$

where r, q, p are pseudothermodynamic parameters. Indeed, while r represents the usual measure of temperature D and $p > 0$ is a constant, the A-dependent parameter q is an unconventional measure of the intensity of active driving. A similar tricritical point appears in the periodically driven mean-field Suzuki-Kubo model of magnetism, which can be interpreted in our terms as a description of the zero tension behavior [68].

The adiabatic approximation fails at low temperatures (small D) where the escape time diverges, and in this range the phase diagram has to be corrected numerically; see Fig. 5(b). By simulating directly Eq. (1), we obtain that even the moderate temperature features of the diagram (tricritical point, point D_e, and the vertical asymptote of the boundary separating phases I and III at large values of A) are captured adequately by the adiabatic approximation. For instance, the value of temperature corresponding to point N (at infinite A) obtained from the adiabatic approximation is $D_N = q/[8(1 + k)]$, where q is a solution of a transcendental equation $q - k =$
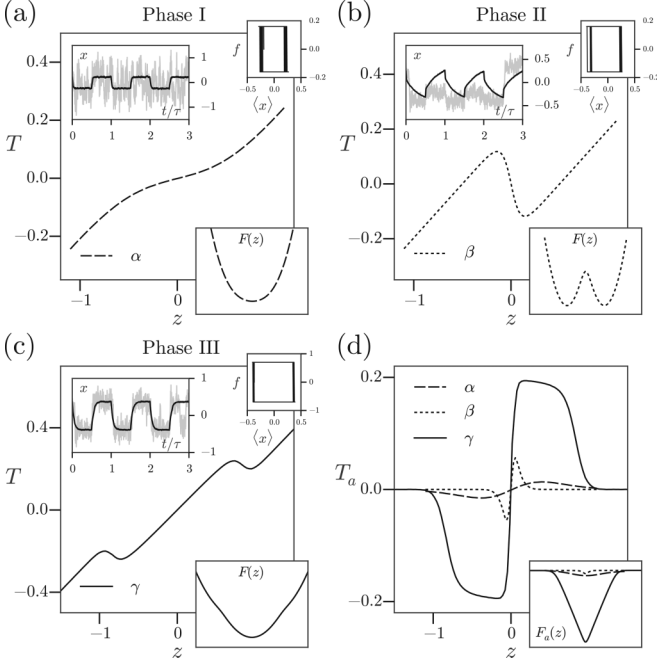
FIG. 6. (a)–(c) Typical tension-length relations in phases I, II, and III. Points α, β, and γ are the same as in Fig. 5(b). Part (d) shows the active component of the force. Insets show the behavior of stochastic trajectories in each of the phases at $z \simeq 0$ (gray lines) superimposed on their ensemble averages (black lines): the stationary hysteretic cycles, the structure of the effective potentials $F(z)$, and the active potential $F_a(z)$ defined as a primitive of the active force $T_a(z)$. The parameters are $k = 0.6$, $\tau = 100$.

$q^{3/2}/\{\sqrt{q} + e^{1/q}\sqrt{\pi}[1 + \mathrm{erf}(1/q)]\}$, which agrees with our numerics; for additional details, see Appendix A.

The new feature of the nonadiabatic phase diagram is a dip of the boundary separating phases II and III at some $D < D_e$ leading to an interesting reentrant behavior (cf. [69,70]). This is an effect of stochastic resonance that is not captured by the adiabatic approximation.

To verify our numerical results in the low-temperature domain $D \to 0$, we used Kramers' approximation, valid when the rocking period τ is much smaller than the typical escape time of the bistable potential V (see Appendix B and Sec. IV for details). It allows one to compute explicitly the location of point K ($A = 1/2$) and point M ($A = 1/2 + k/4$), which we found to be in full agreement with our numerical simulations; see Fig. 5(b). Because of the difference of the limits $D \to 0$ and $\tau \to \infty$, these points are rather far from the corresponding adiabatic predictions K_A and M_A shown in Fig. 5(a).

Force-elongation relations characterizing the mechanical response of the system at different points on the (A,D) plane [Fig. 5(b)] are shown in Fig. 6, where the upper insets illustrate the typical stochastic trajectories and the associated cycles in the $\{\langle x(t) \rangle, f(t)\}$ coordinates. We observe that while in phase I thermal fluctuations dominate periodic driving and undermine the two-well structure of the potential, in phase III the jumps between the two energy wells are fully synchronized with the rocking force. In phase II, the system shows intermediate behavior with uncorrelated jumps between the wells.

In Fig. 6(d) we illustrate the active component of the force $T_a(z) = T(z; A) - T(z; 0)$ in phases I, II, and III. A salient feature of Fig. 6(d) is that active force generation is significant only in the resonant (Kapitza) phase III. A biologically beneficial plateau (tetanus) is a manifestation of the triangular nature of a pseudowell in the active landscape $F_a(z) = \int^z T_a(s)ds$; note also that only a slightly bigger $(f, \langle x \rangle)$ hysteresis cycle in phase III, reflecting a moderate increase of the extracted work, results in a considerably larger active force. It is also of interest that the largest active rigidity is generated in the state $z = 0$, where the active force is equal to zero.

If we now estimate the nondimensional parameters of the model by using the data on skeletal muscles (see Sec. II C), we obtain $A = 0.5$, $D = 0.01$, and $\tau = 100$. This means that muscle myosins in stall conditions (isometric contractions) may be functioning in resonant phase III. Our simple model can therefore contribute to the explanation of the observed stability of skeletal muscles in the negative stiffness regime [19]; a similar mechanism may also be behind the titin-based force generation at long sarcomere lengths [71].

B. Dichotomous (DC) driving

P driving is only one of the correlated signals that can serve as a mechanical representation of an out-of-equilibrium chemical reservoir. To ascertain the robustness of the results obtained in the case of P driving, we now consider another type of correlated forcing that is also characterized by two parameters, namely the amplitude A and the characteristic time τ. It is given by the explicit formula $f(t) = A(-1)^{n(t)}$, where $n(t)$ is a Poisson process with $P(n) = e^{-\lambda}\lambda^n/n!$ with $\lambda = 1/(2\tau)$ and is known as symmetric dichotomous (DC) noise or a random telegraph signal [72,73]. For this Markov process, we have $\langle f(t) \rangle = A \exp(-t/\tau)$ and $\langle f(t), f(s) \rangle = A^2 \exp(-|t - s|/\tau)$.

The probability distribution can be written in the form $p(x,t) = p_-(x,t) + p_+(x,t)$, where $p_\pm(x,t)$ are the probability densities to be in a state x at time t given that $f = \pm A$. The DC driven system (1) is described by the two coupled Fokker-Planck equations [74],

$$\partial_t p_\pm = \partial_x(\partial_x E_\pm p_\pm + D\partial_x p_\pm) + \lambda(\mp p_\pm \pm p_\mp), \quad (11)$$

where $E_\pm(x) = \tilde{V}(x) \mp Ax$. Note that in this interpretation, the DC noise appears as a chemical reaction violating the detailed balance [75]. The stationary version of the system (12) can be written in a transparent form if in addition to $p(x) = p_-(x) + p_+(x)$ we introduce a complimentary variable $d(x) = p_+(x) - p_-(x)$. Then we obtain

$$\partial_x \tilde{V} p - D\partial_x p - Ad = 0,$$
$$\tau \partial_x(\partial_x \tilde{V} d - D\partial_x d - Ap) = d. \quad (12)$$

The numerical study of (1) with DC noise shows that the qualitative structure of the phase diagram in the (A,D) plane remains the same as in the case of P driving; see Fig. 7. We again observe phases I, II, and III and the tricritical point at about the same location as in the case of P noise.

To interpret the numerical results, it is instructive to consider analytically tractable special cases. First of all, Eq. (11) can be used to obtain the adiabatic ($\tau \to \infty$) limit when
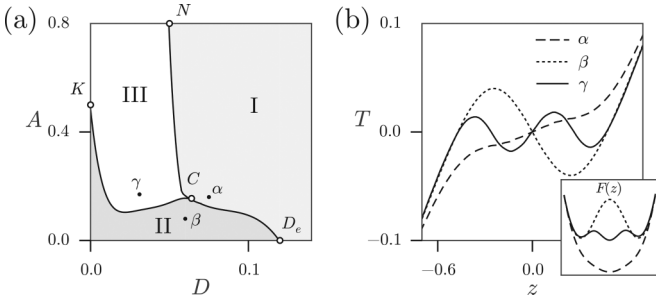
FIG. 7. (a) Phase diagram in the case of DC driving. The identification of phases I, II, and III is the same as in Figs. 5(a) and 5(b). (b) Typical tension-length relations in different phases (b). Here $\tau = 100$ and $k = 0.6$.

FIG. 9. (a) Phase diagram in the case of OU driving. The identification of phases I and II is the same as in Figs. 5(a) and 5(b). (b) The typical tension-length relations in different phases. Here $\tau = 100$ and $k = 0.6$.

the two equations decouple and the steady-state probability distributions take the form $p_\pm(x) \sim \exp[-E_\pm(x)/D]$ as in the case of P driving. The resulting phase diagrams are therefore identical; see Sec. III A. The second case, when the analytic results are available, is the zero-temperature limit $D \to 0$ considered in detail in Sec. IV A. Finally, the third analytically tractable case is $\tau \to 0$, $A \to \infty$, with $\tilde{D} = A^2\tau$ remaining finite. In this limit, we obtain that the nonequilibrium component of the noise is represented by a Gaussian white noise $f(t) = \sqrt{2\tilde{D}}\xi_a(t)$ with the temperature $\tilde{D}$ that is different from the temperature of the equilibrium reservoir D. For instance, one can think about a system exposed to a thermostat with temperature D and a chemostat with temperature $\tilde{D}$. The combined excitations are again represented by a white noise $\sqrt{2D^*}\xi_n(t)$ with effective temperature $D^* = \sqrt{D^2 + \tilde{D}^2}$.

In contrast to the zero-temperature case, now the Kapitza phase III, describing active stabilization, is absent. We obtain only phases I and II separated by a second-order phase transition line $\sqrt{D^2 + \tilde{D}^2} = D_e$ with the universal asymptotic behavior $\tilde{D} \sim (D_e - D)^{1/2}$ near equilibrium; see Fig. 8. The system in this limit can undergo entropic stabilization only, which means that the two-temperature model does not capture the same range of phenomena as the $D = 0$ model. Note that other two-temperature models can exhibit destabilization of a single-well system [51].

C. Ornstein-Uhlenbeck driving

We have seen that the overall effect of the two bounded noises P and DC on a mechanical system may be similar even
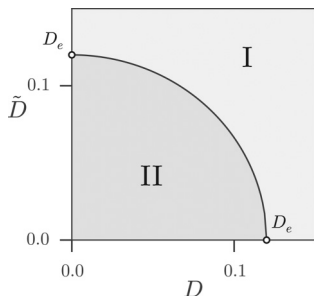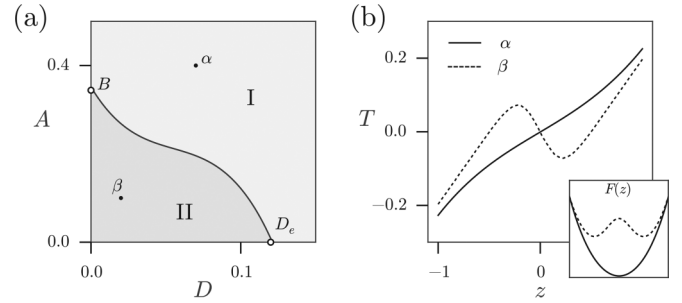

FIG. 8. Phase diagram for the case when the chemical reaction is modeled by an effective temperature $\tilde{D}$. Here $k = 0.6$.

though one of them is highly correlated and non-Markovian and the other is weakly correlated and Markovian. To show that not all noises are "mechanically equivalent," we now consider an Ornstein-Uhlenbeck (OU) process, which is also characterized by two parameters A and τ [73,76].

In the case of OU driving, the function $f(t)$ is a solution of the stochastic equation

$$\frac{df(t)}{dt} = -\frac{1}{\tau}f(t) + A\sqrt{\frac{2}{\tau}}\xi_f(t). \quad (13)$$

As in the case of the DC noise, we have for the first two moments $\bar{f}(t) = \langle f(t) \rangle = A\exp(-t/\tau)$ and $\langle f(s)f(t) \rangle = A^2\exp(-|t-s|/\tau)$, where we assumed for determinacy that $f(0) = A$. The resulting process is also Markovian, however now it is unbounded and is defined on a continuous state space.

The Fokker-Planck equation for the probability density $p(x,f,t)$ takes the form

$$\partial_t p = \partial_x(p\partial_x E + D\partial_x p) + \tau^{-1}\partial_f(fp + A^2\partial_f p). \quad (14)$$

Our numerical results for the system driven by OU noise are summarized in Fig. 9(a). At small intensity of driving A, we observe the conventional picture of entropic stabilization. A striking feature of this diagram is the absence of phase III, which means that in contrast to the cases of P and DC driving, the OU driven system does not support the phenomenon of active stabilization. To understand these numerical results, it is instructive to consider the already mentioned three limiting cases that can be treated analytically.

In the adiabatic limit ($\tau \to \infty$), Eq. (14) simplifies and can be integrated. Then we obtain that $p(x) \sim \exp[-E(x)/D]$, which shows that in this limit only entropic stabilization remains possible.

Another analytically tractable limit is $D \to 0$ (see Sec. IV C), which shows again that in contrast to the cases of P and DC driving, only phases I and II are present at the zero-temperature phase diagram.

Finally, we can consider the double limit $\tau \to 0$, $A \to \infty$, with $\tilde{D} = A^2\tau$ fixed. As in the case of DC noise, we recover in this limit a system subjected to an effective temperature and showing phases I and II only; see Fig. 8.

The analysis of these special cases supports our numerical results suggesting that in the OU-driven system the tricritical point is absent. We can speculate that the failure to generate active rigidity in such a system is due to the unbounded

nature of the OU noise allowing the eventual escape from a neighborhood of any resonant state.

IV. ZERO-TEMPERATURE LIMIT

To understand better the differences between our three representations of nonequilibrium driving, we now compare the behavior of the system in the analytically tractable limit when the temperature of an equilibrium thermostat is equal to zero, $D = 0$. In this limit, the role of passive stabilization is minimized, which allows one to make the effect of active terms more transparent. When $D = 0$, we are left with two nondimensional parameters: the correlation time τ and the amplitude of the active signal A.

A. Dichotomous (DC) driving

In the case of DC driving with $D = 0$, the stationary solution of the Fokker-Plank equation (12) can be written in the form [77]

$$p(x)\partial_x \tilde{V}(x) + A^2 \left[\frac{1}{\tau} - \partial_x (\partial_x \tilde{V}(x) \cdot) \right]^{-1} \partial_x p(x) = 0, \quad (15)$$

where the notation $\partial_x(\partial_x \tilde{V}\cdot)$ should be understood in the sense of differential operators. The formal solution of (15) satisfying zero boundary conditions at infinity can be written in quadratures [66,77],

$$p(x) = \frac{Z^{-1}}{A^2 - [\partial_x \tilde{V}(x)]^2} \exp\left(-\frac{1}{\tau} \int^x \frac{\partial_y \tilde{V}(y)}{A^2 - [\partial_y \tilde{V}(y)]^2} dy \right),$$

where we still need to find the normalizing constant Z. For this solution to be valid, we must also satisfy the inequality

$$|\partial_x \tilde{V}(x)| < A. \quad (16)$$

When $A = 0$, we recover the deterministic case in which condition (16) selects between the points $x_{0,1}(0)$ where the force vanishes; see the precise definition in Appendix A. In principle, the choice depends on the initial condition, but in the limit of vanishing D and large time t, the trajectory $x(t)$ converges to the point minimizing the potential $\tilde{V}$. The resulting tension elongation relation can then be obtained by setting

$$\overline{\langle x \rangle} = \frac{x_0(0) + x_1(0)}{2} + \text{sgn}(z)\frac{x_1(0) - x_0(0)}{2}.$$

The effective energy $F(z)$ emerges as a symmetric two-parabolic bistable potential where $z = 0$ is a singular spinodal point separating the energy wells at $z = \pm 1/2$.

Another simple case is when $\tau \to 0$ with $A^2\tau = \tilde{D}$ remaining finite. In this limit, activity disappears and driving becomes equilibrium with temperature $\tilde{D}$. The steady-state probability distribution is given by $p(x) \sim \exp[-\tilde{V}(x)/\tilde{D}]$ and the effective energy exhibits a transition from phase II to phase I at the critical temperature D_e defined in Sec. III A.

To compute $p(x)$ in the general case, we identify the admissible set, where (16) holds, as $]x_0(-A), x_0(A)[\bigsqcup]x_1(-A), x_1(A)[$, where parameters $x_{0,1}(\pm A)$ are introduced in Appendix A. We can now integrate $p(x)$ on each of

the segments $]x_0(-A), x_0(A)[$ and $]x_1(-A), x_1(A)[$. The result can be written in the form

$$p(x) = C_0 \Psi_0(x)^{[2\tau(1+k)]^{-1}-1} \mathbf{1}_{]x_0(-A),x_0(A)[}(x)$$
$$+ C_1 \Psi_1(x)^{[2\tau(1+k)]^{-1}-1} \mathbf{1}_{]x_1(-A),x_1(A)[}(x), \quad (17)$$

where $\Psi_0(x) = A^2 - [(1+k)x - kz + 1/2]^2$ and $\Psi_1(x) = A^2 - [(1+k)x - kz - 1/2]^2$.

If the domain of definition is connected as in, say, case 2, when $x_0(A) = x_1(-A) = 0$, a continuity condition relates C_0 and C_1:

$$C_0 = Z^{-1}\Psi_1(0)^{[2\tau(1+k)]^{-1}},$$
$$C_1 = Z^{-1}\Psi_0(0)^{[2\tau(1+k)]^{-1}}. \quad (18)$$

If instead either $x_0(A)$ or $x_1(-A)$ is different from zero, the two sets $]x_0(-A), x_0(A)[$ and $]x_1(-A), x_1(A)[$ are separated by a segment where the probability is equal to zero. This means that the passage from one region to the other is impossible. In this case, the coefficients C_0 and C_1 depend on the initial probability distribution as in the periodic case (at $D = 0$). These cases are referred to as cases 1, 3, and 4 in Appendix B.

If we regularize the problem by adding a weak white noise (small $D \neq 0$), the choice of constants again becomes unambiguous as we can associate the support of the distribution with the side (0 or 1) opposite to the smallest potential barrier. We can then write explicitly $C_1 = Z^{-1}\max(0, \text{sgn}(z))$ and $C_0 = Z^{-1} - C_1$. In all cases, the constant Z is found from normalization.

We illustrate the stationary probability distributions $p(x)$ in Fig. 10(a) for several choices of parameters. The analytical expression for the tension elongation curves $T(z)$ involves hypergeometric functions and is too complex to be presented here. The resulting curves are illustrated in Fig. 10 for small and large values of the correlation time. The phase diagram, shown in Fig. 11(a), exhibits all three phases I, II, and III with a tricritical point C' located at $\tau_{C'} = [2(k+1)]^{-1}$ and $\tilde{D}_{C'} = D_e + [2(k+1)]^{-1}/4$. The behavior of the force-elongation relations in different phases is illustrated in Fig. 11(b). As we see, the DC-driven dynamics is sufficiently rich to capture both active and entropic stabilization phenomena even in the absence of the equilibrium reservoir (at $D = 0$).

B. Periodic (P) driving

The numerical simulations for the problem with P driving and $D \to 0$ show only phases II and III even for rapidly oscillating external fields; see Fig. 11(c). To understand this result, we can use Kramers' approximation developed in Appendix B under the assumption that the rocking period is short compared to at least one of the escape times $\tau_{0,1}(\pm A)$. The use of such an antiadiabatic limit is consistent with the observation that in the limit $D \to 0$ the escape times from the energy wells diverge; see Appendix A.

A study of the purely mechanical problem with P driving reveals that, since the potential E can have up to four local minima, the dynamical system (8) can have up to four stationary solutions. In the four cases introduced in
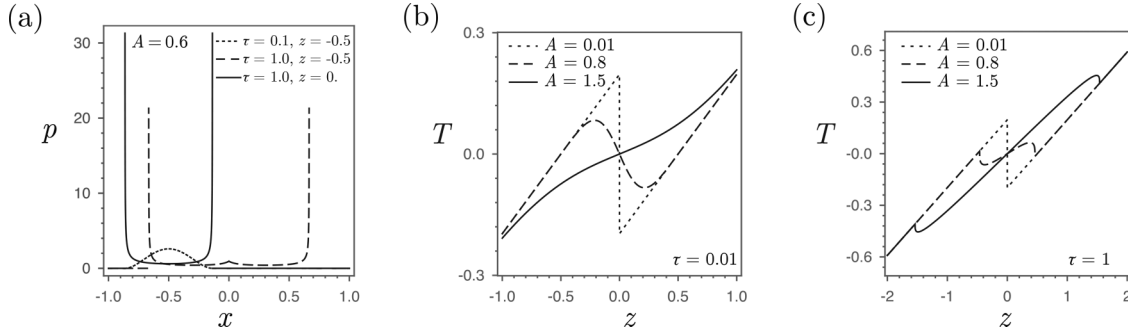
FIG. 10. (a) Examples of stationary probability distributions in the case of DC driving with $A = 0.6$. Dotted line: $\tau = 0.1$, $z = -0.5$. Dashed line: $\tau = 1$, $z = -0.5$. Solid line: $\tau = 1$, $z = 0$. (b),(c) Tension elongation relations for different values of τ.

Appendix B, these solutions give the following:

Case 1: $\overline{\langle x \rangle} = [x_0(-A) + x_0(A)]/2$.
Case 2: $\overline{\langle x \rangle} = [x_0(-A) + x_1(A)]/2$.
Case 3: $\overline{\langle x \rangle} = [x_1(-A) + x_1(A)]/2$.
Case 4:

$$\overline{\langle x \rangle} = \begin{cases} \frac{1}{2}[x_0(-A) + x_0(A)] & \text{if } z < 0, \\ \frac{1}{2}[x_1(-A) + x_1(A)] & \text{if } z > 0. \end{cases}$$

To justify, for instance, the last expression (case 4), we use (B2) to obtain

$$\langle n_0 \rangle \sim e^{(-\min_{\pm A} [\Delta E_1(\pm A)] + \min_{\pm A,1,0} [\Delta E_{0,1}(\pm A)])/D}.$$

Then either $\min_{\pm A} \Delta E_1(\pm A) = \min_{\pm A,1,0} \Delta E_{0,1}(\pm A)$ and $\langle n_0 \rangle = 1$ or $\min_{\pm A} \Delta E_1(\pm A) > \min_{\pm A,1,0} \Delta E_{0,1}(\pm A)$
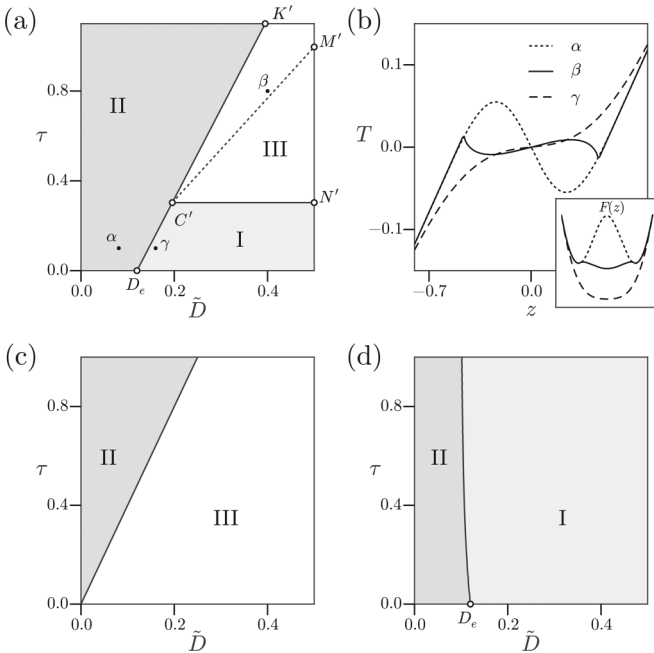

FIG. 11. (a) Zero-temperature phase diagram in the case of DC driving. The identification of phases I, II, and III is the same as in Figs. 5(a) and 5(b). Tension-elongation relations in the case of DC driving in different phases (b). Zero-temperature phase diagram in the case of P driving (c) and OU driving (d). Parameters are $k = 0.6$ and $D = 0$.

and $\langle n_0 \rangle = 0$. The condition $\min_{\pm} \Delta E_1(\pm A) > \min_{\pm,1,0} \Delta E_{0,1}(\pm A)$ introduces the dependence of the stationary distribution on z. In the limit $D \to 0$, the distributions $p_{0,1}(x; \pm A)$ become δ functions concentrated at the points $x_{0,1}(\pm A)$, which gives our formula for $\overline{\langle x \rangle}$.

If we now substitute the values for $x_{0,1}(\pm A)$, given in Appendix A, we obtain the analytic expressions for the tension $T(z)$. Then, by solving the equation $T(z) = 0$, we can locate the line of the first-order phase transition separating phases II and III and show that $A = \frac{1}{2}$ at point K and that $A = \frac{1}{2}(1 + \frac{k}{2})$ at point M, both in agreement with the numerical phase diagram presented in Fig. 12(c). The qualitative difference between the predictions of the adiabatic approximation implying that D is large and the Kramers approximations corresponding to small D is illustrated in Fig. 12.

In coordinates $(\tau, \tilde{D})$, the phase diagram for the P-driven system with zero temperature shows a single phase boundary separating phases II and III; see Fig. 11(c). The entropically stabilized phase II is absent because there is no stochastic contribution allowing the system to cross arbitrary barriers. For the same reason, the phase boundary between phases II and III in the P-driven system is shifted compared to the case of DC driving as the point D_e does not exist anymore. This is in contrast to the fact that at finite D the two systems (with P and DC driving) behave quite similarly. In particular, they are indistinguishable in the adiabatic limit $\tau \to \infty$.

C. Ornstein-Uhlenbeck (OU) driving

In the case of OU driving with $D = 0$, an analytical approximation of the stationary probability distribution is available when $\tau \ll 1$ [66]. The main idea is to combine Eqs. (8) and (13) to obtain a new equation for a noisy inertial oscillator,

$$\frac{d^2 x}{dt^2} + \frac{dx}{dt}[1 + \tau \partial_{xx} \tilde{V}(x)] + \partial_x \tilde{V}(x) = A\sqrt{2\tau}\xi_f(t), \quad (19)$$

where ξ_f is a standard white noise. At large times, the inertial dynamics with additive noise (19) can be approximated by the overdamped dynamics with multiplicative noise,

$$\frac{dx}{dt} = [1 + \tau \partial_{xx} \tilde{V}(x)]^{-1}(-\partial_x \tilde{V}(x) + A\sqrt{2\tau}\xi_f(t)),$$
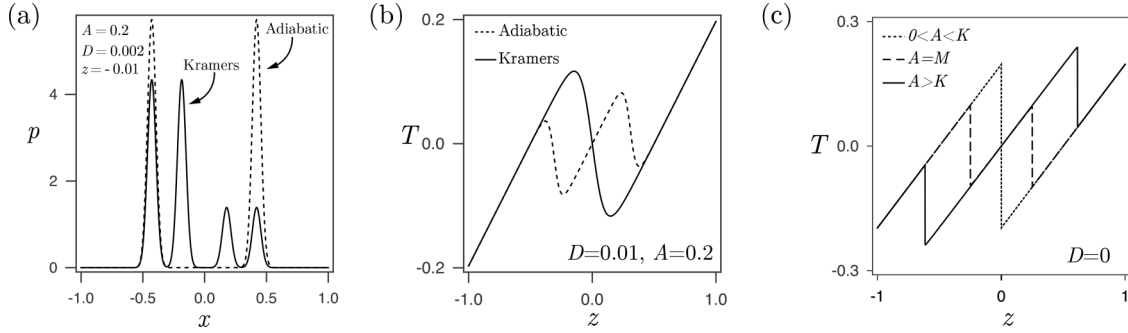
FIG. 12. (a) Examples of the stationary probability distributions in the case of P driving in adiabatic (dotted line) and Kramers (solid line) approximations at $A = 0.2$, $z = -0.01$, $D = 0.002$. (b) Tension elongation relations for $D = 0.01$ and $A = 0.2$ expressed by the Kramers solution (solid line) and the adiabatic solution (dotted line). (c) Tension elongation relations in the limit $D \to 0$ for several value of A. For $0 < A < K$, all curves collapse (dotted line) since the energy injected by the rocking is not sufficient to overcome the potential barriers.

which must be interpreted in the Stratanovitch sense [66]. The corresponding Fokker-Planck equation

$$\partial_t p = \partial_x \left(\frac{\partial_x \tilde{V}}{1 + \tau \partial_{xx} \tilde{V}} p \right)$$
$$+ \partial_x \left[\frac{1}{1 + \tau \partial_{xx} \tilde{V}} \partial_x \left(\frac{A^2 \tau}{1 + \tau \partial_{xx} \tilde{V}} p \right) \right] \quad (20)$$

has an explicit stationary solution [66]:

$$p(x) = Z^{-1} |1 + \tau \partial_{xx} \tilde{V}(x)| \exp \left(-\frac{\tilde{V}(x) + \tau [\partial_x \tilde{V}(x)]^2/2}{A^2 \tau} \right).$$

Notice again that when $\tau \to 0$ with $\tilde{D} = \tau A^2$ fixed, $f(t)$ becomes a white noise and the distribution $p(x)$ takes the classical Boltzmann form.

In Fig. 13(a), we show examples of the stationary distributions for specific values of parameters. The corresponding tension curves $T(z)$ are illustrated in Figs. 13(b) and 13(c) for large and small correlation times.

Figure 11(d) shows the resulting phase diagram, which, as expected, exhibits only phases I and II. This is again a confirmation of the fact that in the case of OU driving, the crucial phase III, describing the phenomenon of active rigidity, is absent. When τ is small (at a fixed $\tilde{D}$), the OU noise becomes a white noise and, as in the case of the DC driving, the phase boundary separating phases I and II passes through the point D_e.

The comparison of all three phase diagrams, shown in Figs. 11(a), 11(c), and 11(d), suggests that at zero temperature the system with DC driving is an intricate *amalgam* of the systems with OU and P driving.

V. CONCLUSIONS

Our model of a molecular device generating *active rigidity* complements the existing models of molecular machines generating *active force*. Instead of a single stall state, we study a family of stall states depending on a parameter, and we quantify the energetic cost of varying this parameter. Since in our case this parameter is mesoscopic strain, the associated derivative of the time-averaged energy is the effective rigidity.

The prototypical model presented in this paper shows that by controlling the degree of nonequilibrium in the system, one can stabilize apparently unstable or marginally stable mechanical configurations, and in this way modify the structure of the effective energy landscape (when it can be defined). The associated pseudoenergy wells with a resonant nature may be crucially involved not only in muscle contraction but also in hair cell gating [14], integrin binding [57], and other internally driven biological and nonbiological phenomena [39–41]. While it is often assumed that the mechanical effect of a nonequilibrium chemical reservoir is a colored noise, our analysis supports the idea that apparently similar noises can generate qualitatively different mechanical effects that may be
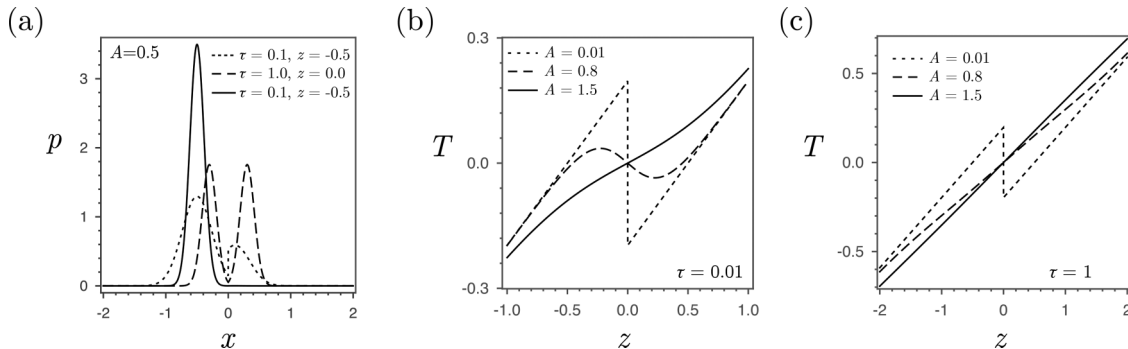

FIG. 13. (a) Examples of stationary probability distributions in the case of OU driving at $A = 0.5$. Dotted line: $\tau = 1$, $z = -0.5$. Dashed line: $\tau = 1$, $z = 0$. Solid line: $\tau = 0.1$, $z = -0.5$. (b),(c) Tension elongation relations in the OU cases for small (b) and large (c) correlation times. Large correlation times are formally outside of the domain of validity of the approximation.

ultrasensitive to the higher order correlations of the stochastic forces.

The experimental verification of the proposed model requires quantitative monitoring of the rigidity of a biological system (say, a cytoskeleton) combined with the control of activity elements (say, molecular motors), and the corresponding experimental techniques are already available [4,44]. The mastery of tunable rigidity will open interesting prospects not only in biomechanics [78] but also in engineering design, incorporating negative stiffness [79] or aiming at synthetic materials involving dynamic stabilization [80,81].

APPENDIX A: ADIABATIC APPROXIMATION FOR SQUARE-SHAPED PERIODIC DRIVING

In the case of biquadratic potential, the driving time scale τ should be compared with the mean exit times from each of the energy wells at both positive and negative values of the tilting force. To find these times, one may consider the four auxiliary potentials (see Fig. 14),

$$E_{0,1}(x,\pm A) = \tilde{V}_{0,1}(x) \mp Ax,$$

where

$$\tilde{V}(x) = \begin{cases} \tilde{V}_0(x) & \text{if } x \leqslant 0, \\ \tilde{V}_1(x) & \text{if } x \geqslant 0. \end{cases}$$

Notice that the bottoms of these quadratic potentials are located at $x_{0,1}(\pm A)$, where

$$x_0(-A) = \min\left(0, \frac{-1/2 + kz - A}{1 + k}\right) \leqslant x_0(A),$$

$$x_0(A) = \min\left(0, \frac{-1/2 + kz + A}{1 + k}\right) \leqslant 0,$$

$$x_1(-A) = \max\left(0, \frac{1/2 + kz - A}{1 + k}\right) \geqslant 0,$$

$$x_1(A) = \max\left(0, \frac{1/2 + kz + A}{1 + k}\right) \geqslant x_1(-A).$$

The four mean exit times $\tau_{0,1}(\pm A)$ can then be written in the form [82]

$$\tau_0(\pm A) = \frac{1}{D}\int_{x_0(\pm A)}^0 e^{\frac{E_0(x;\pm A)}{D}} \int_{-\infty}^x e^{-\frac{E_0(y;\pm A)}{D}} dy\, dx,$$

$$\tau_1(\pm A) = \frac{1}{D}\int_{x_1(\pm A)}^0 e^{\frac{E_1(x;\pm A)}{D}} \int_{\infty}^x e^{-\frac{E_1(y;\pm A)}{D}} dy\, dx.$$

For the adiabatic approximation to work, we need to require that

$$\tau \gg \tau_{0,1}(\pm A).$$

First, it is clear that the adiabatic approximation holds for sufficiently large D because in this case $\tau_{0,1}(\pm A) \to 0$. It also works when $\tau \gg 1$ and $A \gg 1$ as in this case

$$\tau_0(A) = \tau_1(-A) = 0 \quad \text{and}$$

$$\tau_1(A) = \tau_0(-A) \sim \frac{1}{D}\int_{-A}^0 e^{\frac{-Ax}{D}} \int_{-\infty}^x e^{\frac{Ay}{D}} dy\, dx = 1.$$

APPENDIX B: KRAMERS APPROXIMATION FOR SQUARE-SHAPED PERIODIC DRIVING

Here we assume that $\tau \ll \tau_{0,1}(\pm A)$, where the escape times $\tau_{0,1}(\pm A)$ were introduced in Appendix A. With the four potentials $E_{0,1}(\pm A)$ discussed in Appendix A, we associate four activation barriers $\Delta E_{0,1}(\pm A)$. We then distinguish the four cases illustrated in Fig. 14:

Case 1: If $x_1(-A) = 0$ and $x_0(A) < 0$, then $\Delta E_1(-A)$ does not exist.

Case 2: If $x_1(-A) = 0$ and $x_0(A) = 0$, then both $\Delta E_1(-A)$ and $\Delta E_0(A)$ do not exist.

Case 3: If $x_1(-A) > 0$ and $x_0(A) = 0$, $\Delta E_0(A)$ does not exist.

Case 4: If $x_1(-A) > 0$ and $x_0(A) < 0$ and all four barriers exist:

$$\Delta E_0(\pm A) = \frac{(1 \pm 2A - 2kz)^2}{8(1 + k)},$$

$$\Delta E_1(\pm A) = \frac{(1 \pm 2A + 2kz)^2}{8(1 + k)}.$$

We first consider the generic *Case 4*, in which we can apply the rate theory for a rocked bistable system [83,84].
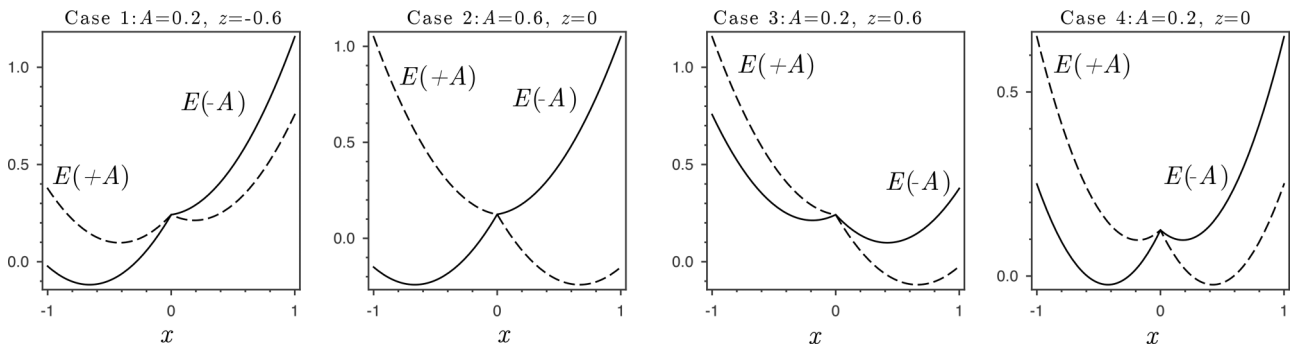

FIG. 14. Four typical potentials $E(\pm A)$. *Case 1*: $x_1(-A) = 0$ and $x_0(A) < 0$; $\Delta E_1(-A)$ does not exist. *Case 2*: $x_1(-A) = 0$ and $x_0(A) = 0$; $\Delta E_1(-A)$ and $\Delta E_0(A)$ do not exist. *Case 3*: $x_1(-A) > 0$ and $x_0(A) = 0$; $\Delta E_0(A)$ does not exist. *Case 4*: $x_1(-A) > 0$ and $x_0(A) < 0$; all four barriers exist.

Denote by $n_0(t)$ the number of particles in the 0 well. When $D \ll \Delta = E_{0,1}(\pm A)$, we can write the reaction equation

$$\dot{n}_0 = -(W_1 + W_0)n_0 + W_1. \tag{B1}$$

Here $W_1(t)$ and $W_0(t)$ are the reaction rates given by [85]

$$W_0(t) = U_0(t)e^{-\frac{[1+2A(-1)^{n(t)}-2kz]^2}{8(1+k)D}}$$

and

$$W_1(t) = U_1(t)e^{-\frac{[1+2A(-1)^{n(t)}+2kz]^2}{8(1+k)D}},$$

where

$$U_0(t) = \frac{1}{2}\sqrt{\frac{(1+k)[1/2 + A(-1)^{n(t)} - kz]}{2\pi D}}$$

and

$$U_1(t) = \frac{1}{2}\sqrt{\frac{(1+k)[1/2 + A(-1)^{n(t)} + kz]}{2\pi D}}.$$

In what follows, we also use the notation $\bar{W} = W_0 + W_1$ and introduce four characteristic times: $W_{0,1}(A) = 1/\tau_{0,1}(A)$ when $n(t)$ is even and $W_{0,1}(-A) = 1/\tau_{0,1}(-A)$ when $n(t)$ is odd. In the limit $\tau\bar{W}(\pm A) \ll 1$ (high-frequency rocking), we can formally average (B1) over a period of the driving force [84] to obtain

$$\frac{d\langle n_0 \rangle}{dt} = -\frac{1}{2}(\bar{W}^+ + \bar{W}^-)\langle n_0 \rangle + \frac{1}{2}(W_1^+ + W_0^-).$$

Then in the steady state,

$$\langle n_0 \rangle = \frac{W_1(A) + W_1(-A)}{\bar{W}(A) + \bar{W}(-A)}. \tag{B2}$$

After time-averaging, the steady-state probability distribution takes the form

$$p(x) = \frac{\langle n_0 \rangle}{2}[p_0(x; -A) + p_0(x; A)]$$
$$+ \frac{1 - \langle n_0 \rangle}{2}[p_1(x; -A) + p_1(x; A)], \tag{B3}$$

where

$$p_0(x; \pm A) = \frac{\exp[-E_0(x; \pm A)/D]}{\int_{-\infty}^{0} \exp[-E_0(x; \pm A)/D]dx},$$

$$p_1(x; \pm A) = \frac{\exp[-E_1(x; \pm A)/D]}{\int_{0}^{\infty} \exp[-E_1(x; \pm A)/D]dx}.$$

Now consider cases 1, 2, and 3 when at least one of the barriers is absent.

Case 1: Each time the rocking flashes to $-A$, all particles that are in the 1 side are drifted toward the 0 side before the rocking flashes to $+A$ again. As both $\Delta E_0(A)$ and $\Delta E_0(-A)$ exist, particles stay much longer to the 0 side, and even if they go the 1 side, they would drift back when the rocking flashes to $-A$ again. So all particles get "ratcheted" to the 0 side, and the stationary (averaged over time) probability reads

$$p_{\text{Kr}}(x) = p_0(x; -A)/2 + p_0(x; A)/2.$$

Case 2: Each time the rocking flashes to $-A$, as $\Delta E_+(-A)$ does not exist, a particle in the 1 gets to the 0 side. In the same way, each time the rocking flashes to $+A$, as $\Delta E_0(A)$ do not exist, a particle in the 0 side gets to the 1 side. The stationary distribution averaged over time reads

$$p_{\text{Kr}}(x) = p_0(x; -A)/2 + p_1(x; A)/2.$$

Case 3: This case is symmetric to case 1. The stationary distribution reads

$$p_{\text{Kr}}(x) = p_1(x; -A)/2 + p_1(x; A)/2.$$

The tension curves for small D can now be computed using the first moment of probability density (B3), $\langle \bar{x} \rangle = \int_{-\infty}^{\infty} x p_{\text{Kr}}(x)dx$.

[1] G. H. Koenderink, Z. Dogic, F. Nakamura, P. M. Bendix, F. C. MacKintosh, J. H. Hartwig, T. P. Stossel, and D. A. Weitz, Proc. Natl. Acad. Sci. (USA) **106**, 15192 (2009).

[2] C. P. Broedersz and F. C. MacKintosh, Rev. Mod. Phys. **86**, 995 (2014).

[3] W. W. Ahmed and T. Betz, Proc. Natl. Acad. Sci. USA **112**, 6527 (2015).

[4] W. W. Ahmed, É. Fodor, and T. Betz, Biochim. Biophys. Acta **1853**, 3083 (2015).

[5] S.-i. Sasa and H. Tasaki, J. Stat. Phys. **125**, 125 (2006).

[6] A. Aminov, Y. Kafri, and M. Kardar, Phys. Rev. Lett. **114**, 230602 (2015).

[7] U. Basu, C. Maes, and K. Netočný, Phys. Rev. Lett. **114**, 250601 (2015).

[8] D. E. Ingber, N. Wang, and D. Stamenović, Rep. Prog. Phys. **77**, 046603 (2014).

[9] P. R. Onck, T. Koeman, T. van Dillen, and E. van der Giessen, Phys. Rev. Lett. **95**, 178102 (2005).

[10] D. A. Fletcher and R. D. Mullins, Nature (London) **463**, 485 (2010).

[11] R. H. Pritchard, Y. Y. S. Huang, and E. M. Terentjev, Soft Matter **10**, 1864 (2014).

[12] P. Ronceray, C. P. Broedersz, and L. Martin, Proc. Natl. Acad. Sci. (USA) **113**, 2827 (2016).

[13] F. Kobirumaki-Shimozawa, T. Inoue, S. A. Shintani, K. Oyama, T. Terui, S. Minamisawa, S. Ishiwata, and N. Fukuda, J. Physiol. Sci. **64**, 221 (2014).

[14] J. Howard and A. Hudspeth, Neuron **1**, 189 (1988).

[15] P. Martin, A. D. Mehta, and A. J. Hudspeth, Proc. Natl. Acad. Sci. (USA) **97**, 12026 (2000).

[16] C. Batters, M. I. Wallace, L. M. Coluccio, and J. E. Molloy, Philos. Trans. R. Soc. London, Ser. B **359**, 1895 (2004).

[17] A. Huxley and S. Tideswell, J. Muscle Res. Cell Motil. **17**, 507 (1996).

[18] A. Vilfan and T. Duke, Biophys. J. **85**, 818 (2003).

[19] M. Caruel, J.-M. Allain, and L. Truskinovsky, Phys. Rev. Lett. **110**, 248103 (2013).

[20] H. Schillers, M. Wälte, K. Urbanova, and H. Oberleithner, Biophys. J. **99**, 3639 (2010).

[21] R. J. Hawkins and T. B. Liverpool, Phys. Rev. Lett. **113**, 028102 (2014).

[22] J. Étienne, J. Fouchard, D. Mitrossilis, N. Bufi, P. Durand-Smet, and A. Asnacios, Proc. Natl. Acad. Sci. (USA) **112**, 2740 (2015).

[23] U. S. Schwarz and S. A. Safran, Rev. Mod. Phys. **85**, 1327 (2013).

[24] E. I. Butikov, J. Phys. A **44**, 295202 (2011).

[25] É. Fodor, K. Kanazawa, H. Hayakawa, P. Visco, and F. van Wijland, Phys. Rev. E **90**, 042724 (2014).

[26] L. R. G. Treloar, *The Physics of Rubber Elasticity* (Oxford University Press, Oxford, 1975).

[27] L. Vočadlo, D. Alfè, M. J. Gillan, I. G. Wood, J. P. Brodholt, and G. D. Price, Nature (London) **424**, 536 (2003).

[28] J. Howard, *Mechanics of Motor Proteins and the Cytoskeleton* (Sinauer, Sunderland, MA, 2001).

[29] L. Marcucci and L. Truskinovsky, Phys. Rev. E **81**, 051915 (2010).

[30] M. Caruel, J. M. Allain, and L. Truskinovsky, J. Mech. Phys. Solids **76**, 237 (2015).

[31] M. Caruel and L. Truskinovsky, arXiv:1510.03011.

[32] G. Puglisi and L. Truskinovsky, J. Mech. Phys. Solids **48**, 1 (2000).

[33] I. Novak and L. Truskinovsky, Math. Mech. Solids **20**, 697 (2015).

[34] P. Reimann, Phys. Rep. **361**, 57 (2002).

[35] C. R. Doering, W. Horsthemke, and J. Riordan, Phys. Rev. Lett. **72**, 2984 (1994).

[36] M. M. Millonas and M. I. Dykman, Phys. Lett. A **185**, 65 (1994).

[37] R. A. Gallardo, O. Idigoras, P. Landeros, and A. Berger, Phys. Rev. E **86**, 051101 (2012).

[38] C. Fogle, J. Rudnick, and D. Jasnow, Phys. Rev. E **92**, 032719 (2015).

[39] L. F. Cugliandolo, D. R. Grempel, and C. A. da Silva Santos, Phys. Rev. Lett. **85**, 2589 (2000).

[40] M. A. Muñoz, F. d. l. Santos, and M. M. T. d. Gama, Eur. Phys. J. B **43**, 73 (2005).

[41] L. Berthier and J. Kurchan, Nat. Phys. **9**, 310 (2013).

[42] R. Sheshka, P. Recho, and L. Truskinovsky, arXiv:1509.02753.

[43] A. F. Huxley and R. M. Simmons, Nature (London) **233**, 533 (1971).

[44] É. Fodor, W. W. Ahmed, M. Almonacid, M. Bussonnier, N. S. Gov, M.-H. Verlhac, T. Betz, P. Visco, and F. van Wijland, arXiv:1511.00921.

[45] A. A. Zaikin, J. Kurths, and L. Schimansky-Geier, Phys. Rev. Lett. **85**, 227 (2000).

[46] J. P. Baltanás, L. Lopez, I. I. Blechman, P. S. Landa, A. Zaikin, J. Kurths, and M. A. F. Sanjuán, Phys. Rev. E **67**, 066119 (2003).

[47] P. S. Landa and P. V. E. McClintock, Phys. Rep. **532**, 1 (2013).

[48] P. Sarkar, A. K. Maity, A. Shit, S. Chattopadhyay, J. R. Chaudhuri, and S. K. Banik, Chem. Phys. Lett. **602**, 4 (2014).

[49] A. P. Solon, J. Stenhammar, R. Wittkowski, M. Kardar, Y. Kafri, M. E. Cates, and J. Tailleur, Phys. Rev. Lett. **114**, 198301 (2015).

[50] J. Bialké, J. T. Siebert, H. Löwen, and T. Speck, Phys. Rev. Lett. **115**, 098301 (2015).

[51] A. Y. Grosberg and J.-F. Joanny, Phys. Rev. E **92**, 032118 (2015).

[52] S. C. Takatori and J. F. Brady, Curr. Opin. Colloid Interface Sci. **21**, 24 (2016).

[53] M. Joyeux and E. Bertin, Phys. Rev. E **93**, 032605 (2016).

[54] B. Dybiec and L. Schimansky-Geier, Eur. Phys. J. B **57**, 313 (2007).

[55] B. Dybiec, E. Gudowska-Nowak, and I. M. Sokolov, Phys. Rev. E **76**, 041122 (2007).

[56] R. Sheshka and L. Truskinovsky, Phys. Rev. E **89**, 012708 (2014).

[57] T. Erdmann and U. S. Schwarz, Phys. Rev. Lett. **92**, 108102 (2004).

[58] M. T. Woodside, C. García-García, and S. M. Block, Curr. Opin. Chem. Biol. **12**, 640 (2008).

[59] A. N. Gupta, A. Vincent, K. Neupane, H. Yu, F. Wang, and M. T. Woodside, Nat. Phys. **7**, 631 (2011).

[60] N. Etemadi and M. Kaminski, Stat. Probabil. Lett. **28**, 245 (1996).

[61] I. I. Blekhman, *Vibrational Mechanics: Nonlinear Dynamic Effects, General Approach, Applications* (World Scientific, Singapore, 2000).

[62] M. Linari, M. Caremani, and V. Lombardi, Proc. Biol. Sci. **277**, 19 (2010).

[63] A. Lewalle, W. Steffen, O. Stevenson, Z. Ouyang, and J. Sleep, Biophys. J. **94**, 2160 (2008).

[64] C. Barclay, R. Woledge, and N. Curtin, Prog. Biophys. Mol. Bio. **102**, 53 (2010).

[65] M. O. Magnasco, Phys. Rev. Lett. **71**, 1477 (1993).

[66] P. Hänggi and P. Jung, in *Advances in Chemical Physics*, edited by I. Prigogine and S. A. Rice (Wiley, Hoboken, NJ,1995), Vol. 89, pp. 239–326.

[67] H. Risken, *The Fokker-Planck Equation* (Springer, Berlin, 1989).

[68] T. Tomé and M. J. de Oliveira, Phys. Rev. A **41**, 4251 (1990).

[69] C. Van den Broeck, J. M. R. Parrondo, and R. Toral, Phys. Rev. Lett. **73**, 3395 (1994).

[70] K. R. Pilkiewicz and J. D. Eaves, Soft Matter **10**, 7495 (2014).

[71] G. Schappacher-Tilp, T. Leonard, G. Desch, and W. Herzog, PloS One **10**, e0117634 (2015).

[72] A. Ichiki, Y. Tadokoro, and M. I. Dykman, Phys. Rev. E **85**, 031106 (2012).

[73] K. H. Nagai, Y. Sumino, R. Montagne, I. S. Aranson, and H. Chaté, Phys. Rev. Lett. **114**, 168001 (2015).

[74] I. Bena, C. Van den Broeck, R. Kawai, and K. Lindenberg, Phys. Rev. E **68**, 041111 (2003).

[75] J. Prost, J.-F. Chauwin, L. Peliti, and A. Ajdari, Phys. Rev. Lett. **72**, 2652 (1994).

[76] R. Bartussek, in *Stochastic Dynamics*, Vol. 484, edited by L. Schimansky-Geier and T. Pöschel (Springer, Berlin, 1997), pp. 68–80.

[77] V. Klyatskin, Radiofiz. **20**, 562 (1977).

[78] G. Puglisi and L. Truskinovsky, Phys. Rev. E **87**, 032714 (2013).

[79] F. Fritzen and D. M. Kochmann, Int. J. Solids Struct. **51**, 4101 (2014).

[80] M. Bukov, L. D'Alessio, and A. Polkovnikov, Adv. Phys. **64**, 139 (2015).

[81] P. Sarkar, A. Shit, S. Chattopadhyay, and S. K. Banik, Chem. Phys. **458**, 86 (2015).

[82] C. Gardiner, *Handbook of Stochastic Methods: For Physics, Chemistry and the Natural Sciences (Springer Series in Synergetics)*, 3rd ed. (Springer, Heidelberg, 2004).

[83] B. McNamara and K. Wiesenfeld, Phys. Rev. A **39**, 4854 (1989).

[84] P. Jung, Phys. Rep. **234**, 175 (1993).

[85] Z. Schuss, *Theory and Applications of Stochastic Processes*, Vol. 170 (Springer, New York, 2010).